Vol 13 No 5, May 2004
1009-1963/2004/13(05)/0737-09

Chinese Physics

© 2004 Chin. Phys. Soc.
and IOP Publishing Ltd

Simulating the time-dependent Ginzburg–Landau equations for type-II superconductors by finite-difference method*

Liao Hong-Yin(廖红印)†, Zhou Shi-Ping(周世平), and Shi Xiao-Yun(施晓蕴)

Department of Physics, Shanghai University, Shanghai 200436, *China*

(Received 7 September 2003; revised manuscript received 18 November 2003)

This article presents numerical solutions of the periodic time-dependent Ginzburg–Landau model for the type-II superconductors by a finite-difference approximation. Both the static and dynamical properties of a single vortex are studied as the external magnetic field varies. Vortex and anti-vortex can coexist and annihilate with time in the case of no external magnetic field, while the vortex will approach a steady state in the presence of magnetic field. We also study vortex dynamical behaviours while pinning centres exist in the sample and find that the pinning site, which has a significant potential to keep the vortex from moving, may trap the vortex.

Keywords: periodic time-dependent Ginzburg-Landau model, finite-difference approximation, vortex dynamics

PACC: 7460E, 7460J, 7490

1. Introduction

In recent years, vortex dynamics in type-II superconductors has been investigated both analytically and numerically, within the framework of time-dependent Ginzburg–Landau (TDGL) theory.[1−6] In fact, the TDGL model, which describes spatiotemporal dynamical behaviours of the order parameter, magnetic field, and supercurrent, is one of the most useful tools for studying the vortex dynamics of superconductors. In Ref.[3], the authors proved the existence of global weak solutions and a global attractor in the TDGL model with L^2 initial data. However, since the TDGL equations are nonlinear partial differential equations coupled to each other, it is extremely difficult to obtain analytical solutions. For this reason, numerical computation appears to be an important and applicable tool. To date, the numerical integration method [5] and finite-element approximation [6] in co-operation with natural boundary conditions have been frequently used.

Although a generic vortex dynamics in a sample can be described by imposing natural boundary conditions, the periodic boundary conditions have to be involved if specific dynamical properties of vortices, such as the vortex dynamics in a sample with periodic defects, are concerned. The purpose of the present work is to present a flexible and robust numerical algorithm, i.e. a finite-difference approximation. This is then applied to the investigation of vortex dynamics in a type-II superconducting sample under periodic boundary conditions. Numerical simulations are performed to visualize the dynamical processes and thus to directly obtain information on the dynamics of the magnetic flux structure without making any of the *ad hoc* electrodynamic assumptions used in previous models.[7,8]

This paper is organized as follows. In Sec.2, we briefly review the TDGL equations and choose a gauge transformation for eliminating the scalar potential. We arrange the finite-difference formulae of the TDGL equations and simulation methods in the Appendix. In Sec.3, starting with the zero-field cooling (ZFC) state, the methods are applied to study the magnetization process of type-II superconductors, and computational results are presented. We examine the time

*Project supported by the National Natural Science Foundation of China (Grant No 60371033) and partly by Shanghai Leading Academic Discipline Program, China.

†E-mail: hhyy_liao@163.com

evolution of the magnetization and observe how the vortex changes. In Sec.4, conclusions of this work are given.

2. TDGL equations and periodic boundary conditions

In this section, we review briefly the TDGL equations, which were developed by Gor'kov and Kopnin,[7]

$$\begin{aligned}&\gamma\left(\hbar\frac{\partial\psi}{\partial t}+\mathrm{i}e_{\mathrm{s}}\phi\psi\right)\\&+\frac{1}{2m_{\mathrm{s}}}\left(\mathrm{i}\hbar\nabla+\frac{e_{\mathrm{s}}}{c}\boldsymbol{A}\right)^2\psi\\&+\alpha\psi+\beta|\psi|^2\psi=0,\qquad(\text{in }\Omega),\end{aligned}\tag{1}$$

$$\begin{aligned}&\nu\left(\frac{1}{c}\frac{\partial\boldsymbol{A}}{\partial t}+\nabla\phi\right)+\frac{c}{4\pi}\nabla\times\nabla\times\boldsymbol{A}\\&+\mathrm{i}\frac{e_{\mathrm{s}}\hbar}{2m_{\mathrm{s}}}(\psi^*\nabla\psi-\psi\nabla\psi^*)\\&+\frac{e_{\mathrm{s}}^2}{m_{\mathrm{s}}c}|\psi|^2\boldsymbol{A}=0,\qquad(\text{in }\Omega),\end{aligned}\tag{2}$$

where $\Omega\subset R^q$, q=2 or 3 (R^q denotes q-dimensional Euclidean space and Ω is a subspace of R^q), represents the region occupied by the superconducting material; e_{s}=2e and m_{s} are the charge and mass, respectively, of the superconducting charge carriers, e is the electron charge; $\hbar$ is *Planck's* constant divided by 2π. The magnetic induction field $\boldsymbol{B}=\nabla\times\boldsymbol{A}$, and the density of superconducting charge carriers $N_{\mathrm{s}}=|\psi|^2$. α and β are the temperature-dependent coefficients appearing in the Ginzburg–Landau free energy. α changes its sign as temperature crosses the critical temperature T_{c}, i.e. $\alpha<0$ for $T<T_{\mathrm{c}}$ and $\alpha>0$ for $T>T_{\mathrm{c}}$. γ is a time relaxation parameter. ν is a positive constant with its value depending on how the dimensionless form is selected. Physically, the parameter ν represents the driving force of the electric field acting on a vortex. We introduce a length scale l and dimensionless spatial and time coordinates $\boldsymbol{x}$ and t, the complex order parameter ψ, the magnetic potential $\boldsymbol{A}$, and the electric potential ϕ according to $\boldsymbol{x}\to l\boldsymbol{x}$, $t\to\gamma\hbar t/|\alpha|$, $\psi\to\sqrt{(|\alpha|/\beta)}\psi$, $\boldsymbol{A}\to\sqrt{(8\pi\alpha^2l^2/\beta)}\boldsymbol{A}$, and $\phi\to(|\alpha|/\gamma e_{\mathrm{s}})\phi$. The Ginzburg–Landau coherence length and the London penetration depth are given by $\xi=\hbar/\sqrt{2m_{\mathrm{s}}|\alpha|}$ and $\lambda=\sqrt{(\beta m_{\mathrm{s}}c^2/4\pi|\alpha|e_{\mathrm{s}}^2)}$, respectively, where c is the speed of light, $\kappa(=\lambda/\xi)$ is the Ginzburg–Landau parameter. In this paper, we choose the length scale l=ξ.

The dimensionless TDGL equations read as

$$\frac{\partial\psi}{\partial t}+\mathrm{i}\phi\psi=\psi-|\psi|^2\psi-\left(\mathrm{i}\nabla+\frac{1}{\kappa}\boldsymbol{A}\right)^2\psi,\quad(\text{in }\Omega),\tag{3}$$

and

$$\begin{aligned}-\sigma\left(\frac{\partial\boldsymbol{A}}{\partial t}+\kappa\nabla\phi\right)=&\nabla\times\nabla\times\boldsymbol{A}+\frac{1}{\kappa^2}|\psi|^2\boldsymbol{A}\\&+\frac{\mathrm{i}}{2}\frac{1}{\kappa}(\psi^*\nabla\psi-\psi\nabla\psi^*),\quad(\text{in }\Omega),\end{aligned}\tag{4}$$

where σ equals $\sigma_n(2\pi\hbar)/(\gamma m_{\mathrm{s}}c^2)$ and it is a positive relaxation constant.[9] σ_n is the normal conductance.

In the above equations, the unknown functions are the order parameter ψ, the magnetic potential $\boldsymbol{A}$ and the electric potential ϕ. In principle, we need one more equation. This could be resolved by fixing a choice of gauge. We can verify that if (ψ, ϕ, $\boldsymbol{A}$) is a triplet of solutions of Eqs.(3) and (4), so is the ($\psi\mathrm{e}^{\mathrm{i}\kappa\theta}$, $\phi-\kappa\theta_t$, $\boldsymbol{A}+\kappa^2\nabla\theta$) for any given smooth function θ. The following transformation:

$$(\psi,\phi,\boldsymbol{A})\to[\psi\mathrm{e}^{\mathrm{i}\kappa\theta},\phi-\kappa\theta_t,\boldsymbol{A}+\kappa^2\nabla\theta]\tag{5}$$

is called gauge transformation. So, we can choose the gauge ϕ=0, and Eqs.(3) and (4) become

$$\frac{\partial\psi}{\partial t}=\psi-|\psi|^2\psi-\left(\mathrm{i}\nabla+\frac{1}{\kappa}\boldsymbol{A}\right)^2\psi,\quad(\text{in }\Omega),\tag{6}$$

and

$$\begin{aligned}-\sigma\left(\frac{\partial\boldsymbol{A}}{\partial t}\right)=&\nabla\times\nabla\times\boldsymbol{A}+\frac{1}{\kappa^2}|\psi|^2\boldsymbol{A}\\&+\frac{\mathrm{i}}{2}\frac{1}{\kappa}(\psi^*\nabla\psi-\psi\nabla\psi^*),\quad(\text{in }\Omega).\end{aligned}\tag{7}$$

It should be noted that the corresponding mathematical problem is not well defined yet without specifying boundary conditions for ψ and $\boldsymbol{A}$. If the domain spans the entire superconductor, the physical boundary conditions are given by the facts that no current flows from the interior of the superconductor across the points where the microscopic field $\nabla\times\boldsymbol{A}$ coincides with the external field. These boundary conditions have been used in Refs.[5, 6, 9]. However, such attempts to simulate an entire superconductor will generally deteriorate resolutions. Otherwise, the computational task to provide sufficient spatio-temporal resolution would be beyond the capacity of the computer available. Therefore, it is common practice to neglect the sample boundary effect. Thus, in such regions that are far away from the boundary of the superconducting sample, the physically relevant variables, e.g., the magnetic field, the current, etc., are, in some sense, *periodic*. The use of a periodic model allows one to

focus on a piece of the sample with a reasonably large dimension over which interesting phenomena vary. As a result, it is practically feasible to examine the fine structure of a vortex with a reasonable amount of computational task.

Several periodic time-independent Ginzburg–Landau models have been used in analysing the phenomena in type-II superconductors.[10−14] The detailed discussion has been reported in Ref.[13]. We use the constraint of fixing the average magnetic induction $\boldsymbol{B}$ by specifying the total flux Φ in a unit cell, and impose the modified version of the two-dimensional periodic boundary conditions [12,13] in order to adapt to our Eqs.(6) and (7):

$$\psi(L_x, y) = \psi(0, y)\exp(\mathrm{i}y\Phi/2L_x),$$
$$\psi(x, L_y) = \psi(x, 0)\exp(-\mathrm{i}x\Phi/2L_y),$$
$$A_x(L_x, y) = A_x(0, y),$$
$$A_x(x, L_y) = A_x(x, 0) - \Phi/2L_x,$$
$$A_y(L_x, y) = A_y(0, y) + \Phi/2L_y,$$
$$A_y(x, L_y) = A_y(x, 0).$$

Here, L_x and L_y are the lengths of the unit cell along x and y directions, respectively; Φ is the total deduced flux with respect to Φ_0 in the unit cell, and Φ_0 ($\equiv \hbar c/2e$) is the flux quantum. In our simulations, we choose $\Phi = 2\pi n$ with n being a positive integer.

3. Computational results

We now present the numerical simulations using the TDGL model based on the finite-difference approximation described in the Appendix. We choose the parameter σ equal to 10. In fact, a different σ leads only to the variation in the amplitude of ψ and $\boldsymbol{A}$, but the vortex distribution remains unchanged. As to the initial condition, we assume a perfect superconducting state with a proper phase of the order parameter throughout Ω, namely $\psi_0 = ((x - x_0)/\sqrt{(x - x_0)^2 + (y - y_0)^2}, (y - y_0)/\sqrt{(x - x_0)^2 + (y - y_0)^2})$ and $\boldsymbol{A}_0$=0, where (x_0, y_0) is the centre of the cell.[15] Since a uniform magnetic field is applied and there are no external currents or voltages applied to the sample, the vortices will finally approach to a steady-state configuration from a transient state, as time grows.

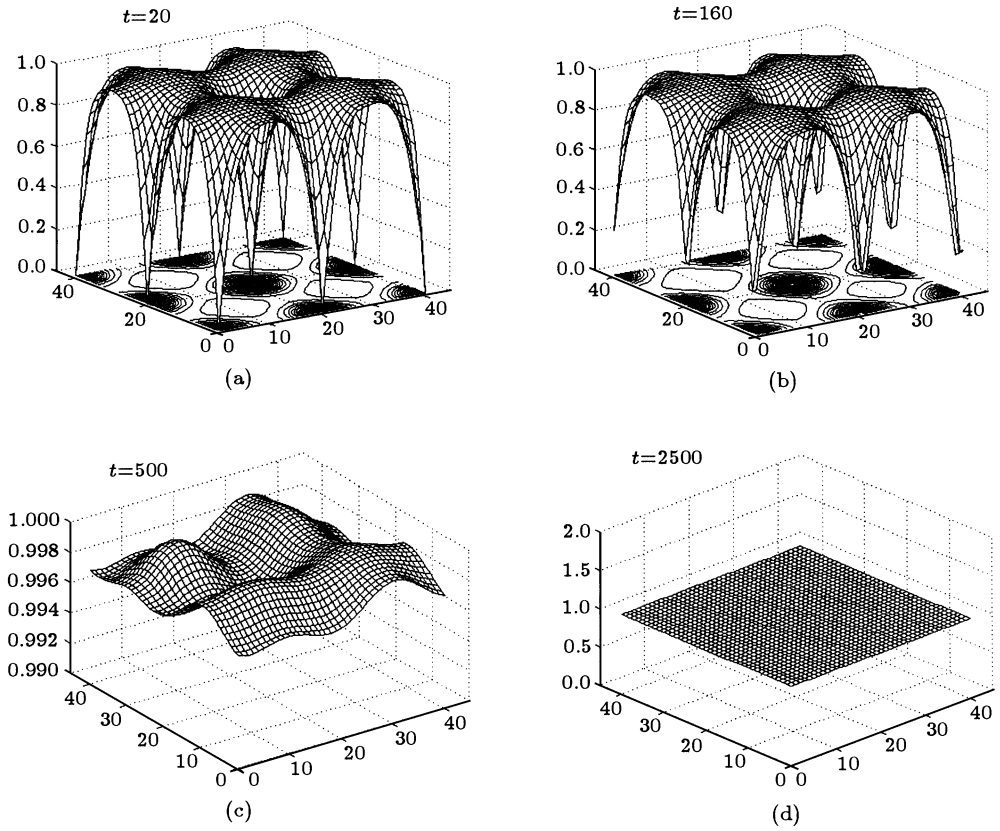


Fig.1. Time evolution of the spatial pattern of $|\psi|$ in Φ=0. The parameters are $N_x = N_y$=40, κ=20, $L_x = L_y$ =20, Δt=0.005.

Firstly, we study the case of $\boldsymbol{H}$=0, namely the magnetic flux Φ=0. In this case, Serfaty [16] proved that, as thermal noise is involved, there exists a superheating field $\boldsymbol{H}_{\rm sh}$ where the stable solution of the Ginzburg–Landau equation is vortexless for $\boldsymbol{H} \leq \boldsymbol{H}_{\rm sh}$, while the Meissner state solution becomes unstable for $\boldsymbol{H} > \boldsymbol{H}_{\rm sh}$ and the vortex and anti-vortex will appear and coexist. Here, the thermal fluctuations are not taken into account, so a $|\psi|$=1 configuration is known to be stable.[17] In Figs.1 and 2, the time evolutions of $|\psi|$ and $\boldsymbol{B}$ are shown, respectively. As expected, the system asymptotically approaches the steady state, namely $|\psi|$=1 and $\boldsymbol{B}$=0, as shown in Figs.1(d) and 2(d), respectively. But in the transient state, there appear localized magnetic field configurations consisting of positive vortex (upward direction) and anti-vortex (downward direction). The flux of each vortex or anti-vortex configuration is quantized, namely $\Phi = \pm 2\pi$. It is apparent that the total flux is equal to zero at an arbitrary instant. We also find that the vortices and anti-vortices attract each other and annihilate eventually, leading the system to a uniform steady state of $|\psi|$=1 as time steadily proceeds. The reason why the superconducting state is gradually accompanied by the nucleation of vortices and anti-vortices is perhaps due to the phase fluctuation of the order parameter that occurs more easily than the amplitude fluctuation. Analytical solution for the steady state is readily obtained, if the vector potential $\boldsymbol{A}$ is completely neglected, but the vortex–antivortex transient-state will be missed, which becomes serious as the thermal fluctuation becomes stronger.

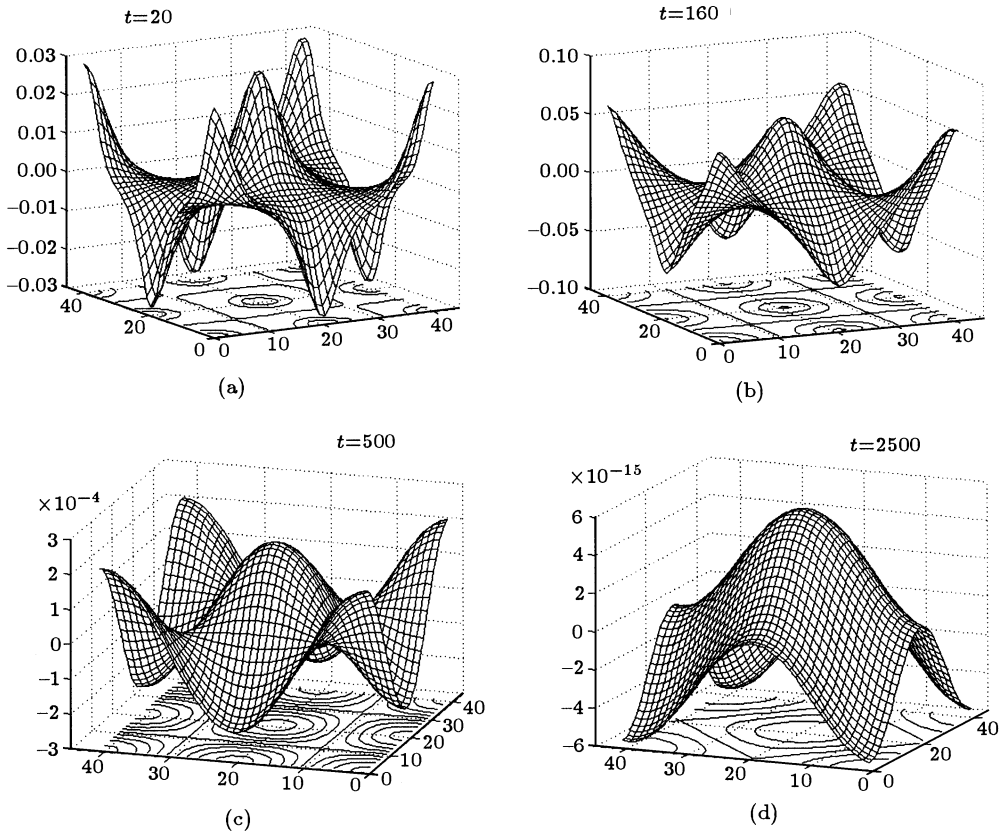


Fig.2. Same as Fig.1, but for B.

Next, we apply a uniform magnetic field to the sample. Tang and Wang [3] have proved that the Ginzburg–Landau system for a superconductor admits a global attractor, which represents exactly all the long-time dynamic behaviours of the system. So, in this case, the vortex state will grow first and asymptotically approaches to an equilibrium state, embedded in the global attractor. In the case of $\Phi = 2\pi$, the equilibrium state is a single vortex state shown in Fig.3. We can visualize the fine structure of a vortex at any instant and its dynamical process leading to regularization, in contrast to that presented in Ref.[6], which has described the dynamics of a vortex lattice and obtained the general property. If we increase Φ

to 4π, there appear several vortices distributing in the sample, as depicted in Fig.4. The vortex distributed in an equilibrium state is similar to the Abrikosov vortex lattice, which is regular and stable. Moreover, the supercurrent $\boldsymbol{J} = \nabla \times \boldsymbol{B}$ distribution in the cell is plotted in Fig.4(c). It indicates that the current approaches to zero either in or far from the centre of a vortex. We also notice that the order parameter, magnetic field and supercurrent are all isotropic because no other perturbation, for example, defects, etc, has been involved.

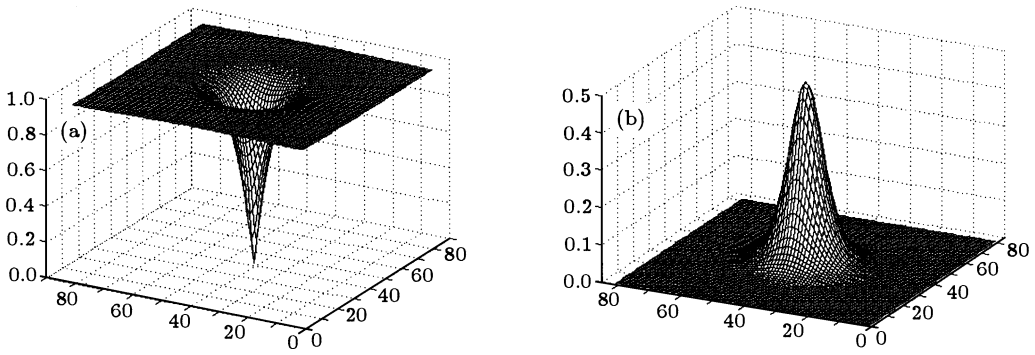


Fig.3. Steady-state distribution for the single vortex state at time t=200: (a) for $|\psi|$ and (b) for $\boldsymbol{B}$. The parameters are $N_x = N_y$=80, κ=20, $L_x = L_y$ =20, Δt =0.005, and $\Phi = \pi$.

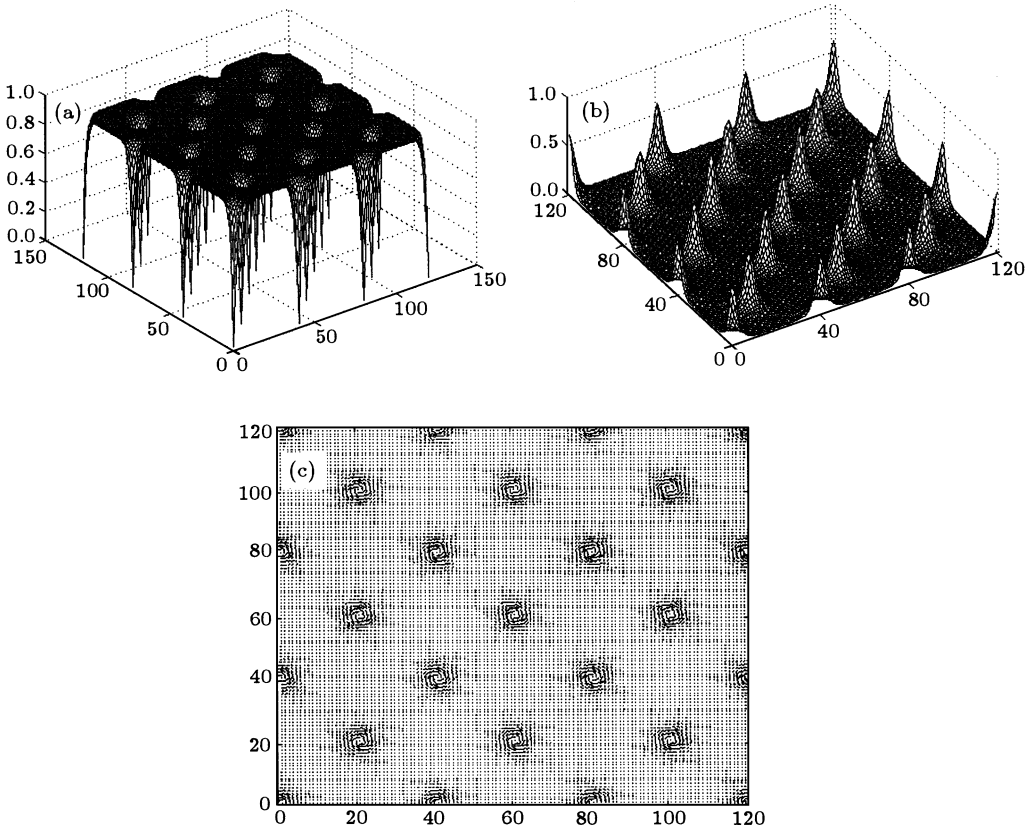


Fig.4. The static distribution of two vortices per unit cell at time t=1000: (a) for $|\psi|$, (b) for $\boldsymbol{B}$ and (c) for $\boldsymbol{J}$. The parameters are $N_x = N_y$=40, κ=2.0, $L_x = L_y$=20, Δt=0.01, and $\Phi = 4\pi$.

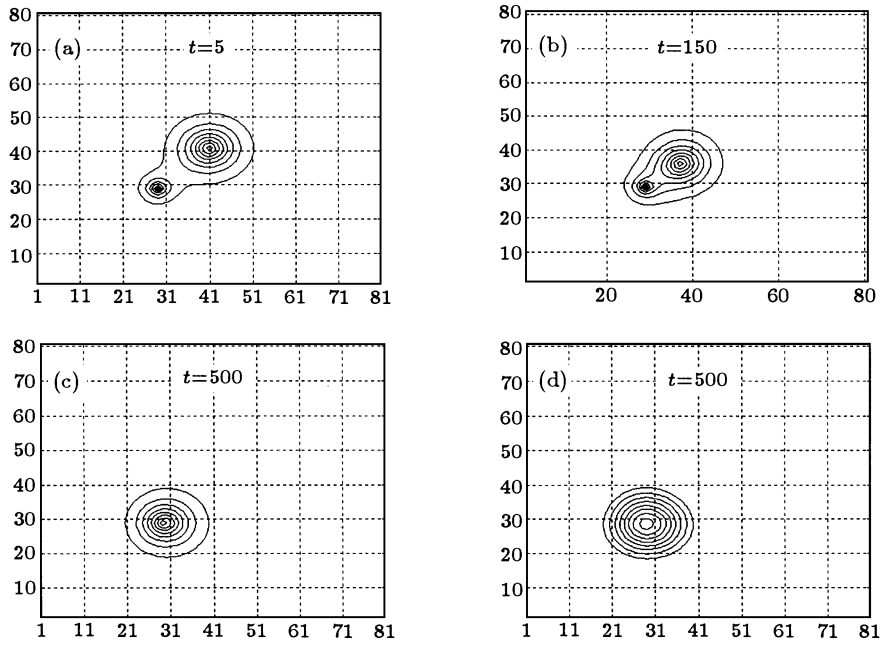


Fig.5. Time evolution of $|\psi|$ at t=5 (a), 150 (b), and 500 (c). Steady-state single vortex distribution is realized at time t=500 and (d) is for $\boldsymbol{B}$. The pinning point is located at (30,30). The parameters are $N_x = N_y$=80, κ=2.0, $L_x = L_y$ =20, Δt=0.01.

Finally, we study the effects of pins on the vortex motion. Since a defect acts effectively on a vortex only within the pinning range, we assume that the pinning force at the pinning sites gives a short-range attractive parabolic potential well.[18] Suppose a single vortex, which is located at the centre of a unit cell. Nearby it, there is a pinning-centre, where the amplitude of an order parameter is assigned to being null. As time increases, the vortex will move toward the pinning site and will be trapped there so that a lowest free energy of the system is realized. The time evolution of $|\psi|$ and $\boldsymbol{B}$ is shown in Fig.5. Furthermore, if there are several pins, they will generate an effective potential well and exert a resultant force to the vortex and affect its movement. If the action from the nearest pinning site dominates over others, the vortex will move to the nearest pinning site, from which the pinning force acting on the vortex is stronger than others, as shown in Fig.6. We also find that the vortex distorts when it moves to the pinning centre because of competition between pinning centres. However, due to the defect which is believed to be azimuthally isotropic and homogeneous, the steady-state vortex pinned precisely on the defect must have a uniform distribution azimuthally, see Figs.5(c) and (d), for instance. This result is consistent with the calculation given in Ref.[8]. During our simulations, we find the distance between a vortex and a pinning centre (site) Δr (in units of ξ) is very important. Beyond a critical distance Δr_c, the time spent in arriving at a steady state is drastically long, which implies that the defect is unable to pin the vortex. This case indicates that a point defect acts effectively on a vortex only within a limited pinning range, which is estimated to be about the radius of the parabolic potential well specified by the defect. We turn to the case of a sample with periodic defect arrays. Recently, flux pinning by well-defined artificial periodic pinning arrays, i.e. triangular or square arrays, in a superconducting film, has been discussed.[18,19] Striking peaks in the magnetization and critical $\boldsymbol{J}_c$ are observed. These peaks are believed to arise from the greatly enhanced pinning that occurs when parts of the vortex lattice become commensurate with (i.e. match) the existing periodic pinning arrays. Under such conditions, extremely stable vortex configurations are generated, which persist under an increasing current or external field.[22] Here, we apply our method to simulate the vortex dynamics in a pinning array and obtain the 'matching field'. Since the pinning site acts as a short-range attractive parabolic well, the system can be modelled as a periodic-type potential well array. As stated above, we set ψ=0 at the pinning sites by solving Eqs.(11)–(13) under periodic boundary conditions. The static distribution is shown in Fig.7. The vortices (the circles) are all trapped by the pinning sites (the asterisks) form-

ing a triangular (Fig.7(a)) or squared (Fig.7(b)) vortex lattices. This case is referred to as the 'matching field effect' given in Ref.[21], in which large-scale simulated annealing as well as flux-gradient-driven molecular dynamics was considered.

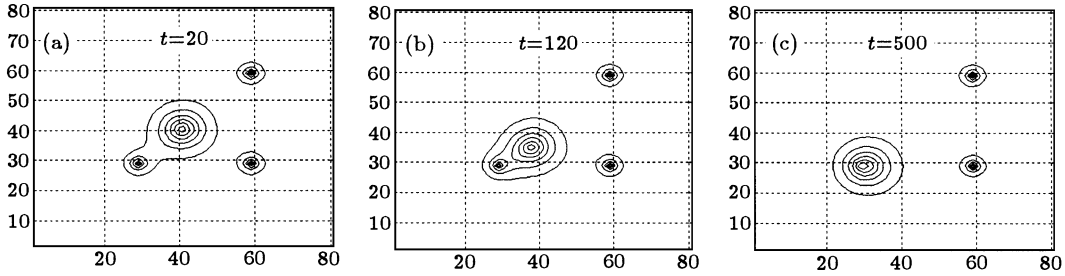


Fig.6. Time evolution of $|\psi|$. Steady-state single vortex distribution is realized at time t=500. There are three pinning points: (30,30), (60,30), (60,60). The parameters are $N_x = N_y$=80, κ=20, $L_x = L_y$ =20, Δt=0.005.

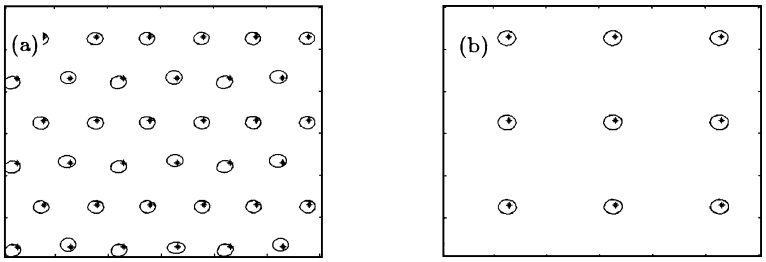


Fig.7. The steady distribution of vortices which are trapped by periodic pinning arrays at time t=1000: (a) for triangular array (Φ=72π); (b) for square array (Φ=18π). The parameters are $N_x = N_y$=120, κ=2.0, $L_x = L_y$ =60, Δt=0.01.

4. Conclusions

In this paper, we have presented and used a finite-difference method to investigate the dynamics of magnetic flux in a periodic TDGL model for type-II superconductors. We simulate the time evolution of the superconducting state by varying with external magnetic field in a two-dimensional sample. We have also studied the interaction between vortices and pins. It is shown that if there are no additional external factors, such as external current, voltage or alternating magnetic field, a single vortex will approach to a steady state from a transient state in which vortices and anti-vortices coexist if no external field has been applied. A defect, which is assumed to be a non-superconducting site, will trap a vortex so as to yield the lowest free energy of the system. In periodic pinning arrays, regular vortex lattices will form depending on the average magnetic field or the total magnetic flux in a unit cell and the geometry of the pinning array.

On solving the TDGL models, we have considered the periodic boundary condition. It is applicable only when no other external driving force exists or the driving force approximately satisfies the periodic conditions. It is the periodic boundary conditions that specify the number of flux quanta in a unit cell, and thus impose another constraint on the flux line motion. In contrast to the natural boundary conditions, by which the generic dynamics in a sample can be observed, the periodic boundary conditions can be applied to the study of specific dynamical properties of a vortex. So, the two conditions complement each other.

In computations, our method is efficient not only in the large-κ case but also in the low-κ case. The numerical error ε is kept within an order of 10^{-8}–10^{-9}, and in some cases even of 10^{-11}, even if the time step is chosen to be relatively large, for instance 10^{-3}–10^{-2}. Therefore, we come to the conclusion that our method is not only convenient and simple, but also mathematically robust and quickly convergent on the full and indispensable condition that the gridding ratio is not more than 1/4, namely $r(=\Delta t/\min((\Delta x)^2+(\Delta y)^2))\leq 1/4$.

Appendix: Finite-difference discretization to TDGL equations

We consider a thin film of a type-II superconductors ($\kappa > 1/\sqrt{2}$) in the $x-y$ plane with a magnetic

field in the z direction, $\boldsymbol{H}$ (0,0,H). We are interested in the field configuration invariant along the z-axis, thus the field depends only on the coordinates x and y, and the third component of the magnetic potential is always zero, that is $\boldsymbol{A} = (A_x, A_y, 0)$. This situation may be physically realized if the thickness of the film, d, is much greater than the coherence length ξ and less than the penetration depth λ.

Now, we discretize the TDGL equations in a rectangular unit cell $L_x \times L_y$, containing $N_x \times N_y$ lattice points. For the parabolic partial-differential equations (6) and (7), we choose a five-point stencil scheme to discretize the spatial derivatives [20] and the predictor–corrector trapezoidal Euler scheme approximation in time is considered. Both cases are then second-order accurate schemes: namely, the interpolation error is in the order of $O((\Delta x)^2+(\Delta y)^2+(\Delta t)^2)$. We can rewrite Eqs.(6) and (7) in scalar form:

$$\begin{aligned}\frac{\partial\psi}{\partial t} =&\psi - |\psi|^2\psi - \left(- \left(\frac{\partial^2\psi}{\partial x^2} + \frac{\partial^2\psi}{\partial y^2}\right) + \mathrm{i}\frac{1}{\kappa}\left(\frac{\partial A_x}{\partial x} + \frac{\partial A_y}{\partial y}\right)\psi \right.\\ &\left. + 2\mathrm{i}\frac{1}{\kappa}\left(A_x\frac{\partial\psi}{\partial x} + A_y\frac{\partial\psi}{\partial y}\right) + \frac{1}{\kappa^2}(A_x^2 + A_y^2)\psi\right), \qquad (8)\\ \frac{\partial A_x}{\partial t} =&-\frac{1}{\sigma}\left(\left(\frac{\partial^2 A_y}{\partial x\partial y} - \frac{\partial^2 A_x}{\partial y^2}\right) + \frac{1}{\kappa^2}|\psi|^2 A_x + \frac{\mathrm{i}}{2}\frac{1}{\kappa}\left(\psi^*\frac{\partial\psi}{\partial x} - \psi\frac{\partial\psi^*}{\partial x}\right)\right), \qquad (9)\\ \frac{\partial A_y}{\partial t} =&-\frac{1}{\sigma}\left(\left(\frac{\partial^2 A_x}{\partial x\partial y} - \frac{\partial^2 A_y}{\partial x^2}\right) + \frac{1}{\kappa^2}|\psi|^2 A_y + \frac{\mathrm{i}}{2}\frac{1}{\kappa}\left(\psi^*\frac{\partial\psi}{\partial y} - \psi\frac{\partial\psi^*}{\partial y}\right)\right). \qquad (10)\end{aligned}$$

The discretized or finite-difference forms are given by

$$\begin{aligned}\psi_{i,j}^{k+1} =&\psi_{i,j}^k + \Delta t\left(\left(\frac{\psi_{i+1,j}^k + \psi_{i-1,j}^k - 2\psi_{i,j}^k}{(\Delta x)^2} + \frac{\psi_{i,j+1}^k + \psi_{i,j-1}^k - 2\psi_{i,j}^k}{(\Delta y)^2}\right)\right.\\ &-\mathrm{i}\frac{1}{\kappa}\left(\frac{Ax_{i+1,j}^k - Ax_{i-1,j}^k}{2\Delta x} + \frac{Ay_{i,j+1}^k - Ay_{i,j-1}^k}{2\Delta y}\right)\psi_{i,j}^k\\ &-2\mathrm{i}\frac{1}{\kappa}\left(Ax_{i,j}^k\frac{\psi_{i+1,j}^k - \psi_{i-1,j}^k}{2\Delta x} + Ay_{i,j}^k\frac{\psi_{i,j+1}^k - \psi_{i,j-1}^k}{2\Delta y}\right)\\ &\left.-|\psi_{i,j}^k|^2\psi_{i,j}^k + \left(1 - \frac{1}{\kappa^2}((Ax_{i,j}^k)^2 + (Ay_{i,j}^k)^2)\right)\psi_{i,j}^k\right), \qquad (11)\\ Ax_{i,j}^{k+1} =&Ax_{i,j}^k + \Delta t\left(-\frac{1}{\sigma}\right)\left(\frac{\mathrm{i}}{2}\frac{1}{\kappa}\left(\psi_{i,j}^{*k}\frac{\psi_{i+1,j}^k - \psi_{i-1,j}^k}{2\Delta x} - \psi_{i,j}^k\frac{\psi_{i+1,j}^{*k} - \psi_{i-1,j}^{*k}}{2\Delta x}\right) + \frac{1}{\kappa^2}|\psi_{i,j}^k|^2 Ax_{i,j}^k\right.\\ &\left.-\left(\frac{Ax_{i,j+1}^k + Ax_{i,j-1}^k - 2Ax_{i,j}^k}{(\Delta y)^2} - \frac{1}{4}\frac{Ay_{i+1,j+1}^k - Ay_{i-1,j+1}^k - Ay_{i+1,j-1}^k + Ay_{i-1,j-1}^k}{(\Delta x\Delta y)}\right)\right), \qquad (12)\\ Ay_{i,j}^{k+1} =&Ay_{i,j}^k + \Delta t\left(-\frac{1}{\sigma}\right)\left(\frac{\mathrm{i}}{2}\frac{1}{\kappa}\left(\psi_{i,j}^{*k}\frac{\psi_{i,j+1}^k - \psi_{i,j-1}^k}{2\Delta y} - \psi_{i,j}^k\frac{\psi_{i,j+1}^{*k} - \psi_{i,j-1}^{*k}}{2\Delta y}\right) + \frac{1}{\kappa^2}|\psi_{i,j}^k|^2 Ay_{i,j}^k\right.\\ &\left.-\left(\frac{Ay_{i+1,j}^k + Ay_{i-1,j}^k - 2Ay_{i,j}^k}{(\Delta x)^2} - \frac{1}{4}\frac{Ax_{i+1,j+1}^k - Ax_{i-1,j+1}^k - Ax_{i+1,j-1}^k + Ax_{i-1,j-1}^k}{(\Delta x\Delta y)}\right)\right), \qquad (13)\end{aligned}$$

where $i = 0, 1, \ldots, N_x$, $j = 0, 1, \ldots, N_y$, $k = 0, 1, \ldots$. At each lattice point (i, j), k is an integer labelling the generations of iteration in time. Thus, $t = k\Delta t$.

In order to solve the nonlinear systems of algebraic equations (12)–(14), we introduce the predictor–corrector trapezoidal Euler scheme,[21]

$$\begin{cases}\text{predictor} & \overline{y}_{n+1} = y_n + hf(x_n, y_n),\\ \text{corrector} & y_{n+1} = y_n + \dfrac{h}{2}\big[f(x_n, y_n) + f(x_{n+1}, \overline{y}_{n+1})\big]\end{cases} \qquad (14)$$

which retains a second-order accuracy in time step. Note that the gauge invariance remains in the modified Euler scheme (for details see for instance Ref.[22]).

We define numerical error ε to be

$$\max\big(|\psi_{i,j}^{k+1} - \psi_{i,j}^k|, |A_{xi,j}^{k+1} - A_{xi,j}^k|, |A_{yi,j}^{k+1} - A_{yi,j}^k|\big), \qquad (15)$$

where (i, j) sweeps all grid points in a unit cell.

It should be noted that, mathematically, coupled nonlinear partial differential equations have more than one solution. It has been proven that a physically relevant solution can be attained as k increases if the iteration starts from a proper initial state (for details see for instance Ref.[15]).

References

[1] Fram H, Ullah S and Dorsey A T 1991 *Phys. Rev. Lett.* **66** 3067

[2] Liu F, Mondello M and Goldenfeld N 1991 *Phys. Rev. Lett.* **66** 3071

[3] Tang Q and Wang S 1995 *Physica* D **88** 139

[4] Du Q 1994 *Appl. Anal.* **52** 1

[5] Kato R, Enomoto Y and Maekawa S 1993 *Phys. Rev.* B **47** 8016

[6] Du Q, Gunzburger M D and Peterson J S 1995 *Phys. Rev.* B **51** 16194

[7] Gor'kov L and Kopnin N 1974 *Sov. Phys. JETP* **38** 195

[8] Friesen M and Muzikar P 1997 *Phys. Rev.* B **55** 509

[9] Du Q 1999 *SIAM J. Appl. Math.* **59(4)** 1225

[10] Doria M M, Gubernatis J E and Rainer D 1990 *Phys. Rev.* B **41** 6335

[11] Wang Z D and Hu C R 1991 *Phys. Rev.* B **44** 11918

[12] Du Q, Gunzburger M D and Peterson J S 1992 *SIAM Review* **34** 54

[13] Kaper H G and Kwong M K 1995 *J. Comput. Phys.* **119** 120

[14] Niu J H, Zhou S P and Xu K X 1998 *Acta Phys. Sin.* **47** 985 (in Chinese)

[15] Zhou S P 2001 *Chin. Phys.* **10** 541

[16] Serfaty S 1999 *Arch. Rational Mech. Anal.* **149** 329

[17] Tinkham M 1975 *Introduction to Superconductivity* (New York: McGraw-Hill)

[18] Reichhardt C, Olson C J and Nori F 1998 *Phys. Rev.* B **57** 7937

[19] Baert M *et al* 1995 *Phys. Rev. Lett.* **74** 3269

[20] Xu C F 1990 *Numerical Solution of Practical Partial Differential Equations* (Wuhan: HuaZhong University of Technology Press, China)

[21] Shen J H *et al* 1998 *Elementary Numerical Analysis* (Shanghai: Tongji University Press, China)

[22] Du Q 1998 *Math. Comp.* **67** 965